Water Mass Transformation by Cabbeling and Thermobaricity

Sjoerd Groeskamp,[1] Ryan P Abernathey,[1] and Andreas Klocker[2]

[1]Columbia University, Lamont-Doherty Earth Observatory, New York, United States of America

[2]Institute for Marine and Antarctic Studies, University of Tasmania, Hobart, Tasmania, Australia

This article has been accepted for publication and undergone full peer review but has not been through the copyediting, typesetting, pagination and proofreading process, which may lead to differences between this version and the Version of Record. Please cite this article as doi: 10.1002/2016GL070860

Water mass transformation is an important process for the global ocean circulation. Nonlinearities in the equation of state of seawater lead to water mass transformation due to cabbeling and thermobaricity. Here, the contribution of cabbeling and thermobaricity to water mass transformation is calculated in a Neutral Density framework, using temperature gradients derived from observationally-based gridded climatologies and observationally-based estimates of the spatially varying eddy diffusivities. It is shown that cabbeling and thermobaricity play a significant role in the water-mass transformation budget, with cabbeling having a particularly important role in the formation of Antarctic Intermediate Water and Antarctic Bottom Water. A physical hypothesis is presented which explains why cabbeling is important for Antarctic Intermediate Water formation. It is shown that spatially varying estimates of eddy diffusivities are essential to correctly quantify the role of cabbeling to the formation of Antarctic Intermediate Water.

Key points:

- Cabbeling is important for AAIW, NADW and AABW formation.
- New AAIW formation mechanism proposed.
- Spatially varying estimates of eddy diffusivities are essential for accurate estimates of water mass transformation.

1. Introduction

The global ocean circulation plays a key role for the ocean's uptake, redistribution and storage of heat, freshwater and biogeochemical tracers, thereby influencing the global climate system. An important component of the ocean circulation is water mass transformation (WMT), which here is defined as the change in a fluid parcel's density as result of changes in Absolute Salinity S_A [g kg^{-1}, *McDougall et al.*, 2012], and changes in the heat content, which is proportional to Conservative Temperature Θ [K, *McDougall*, 2003]. Such changes can be driven by boundary fluxes, such as surface heat and freshwater fluxes, or by mixing, as for example that resulting from stirring by mesoscale eddies.

The nonlinear equation of state (EOS) of seawater leads to some exotic forms of WMT. In particular, cabbeling and thermobaricity are both a consequence of a combination of eddy mixing and nonlinearities in the EOS [*McDougall*, 1984, 1987a]. Cabbeling is the process in which the mixing of two water parcels with different Θ and S_A, but equal density, results in a water parcel denser than the two original water parcels. Thermobaricity is the process in which the mixing of two water parcels with different Θ and pressure (P), but equal density, results in a water parcel which is either lighter or denser than the two original water parcels. Hence both these processes can occur when mesoscale eddies mix Θ and S_A along isopycnal surfaces.

Ocean modeling studies have shown that the contribution from the Nonlinear Equation of State (NEOS) to WMT is in fact significant [*Marsh*, 2000; *Iudicone et al.*, 2008a; *Urakawa and Hasumi*, 2012; *Hieronymus*, 2014]. More specifically, *Nycander et al.* [2015] showed in a coarse-resolution numerical model, in which eddy mixing is parameterised,

that cabbeling is essential for the formation of Antarctic Intermediate Water (AAIW), and *Thomas and Shakespeare* [2015] used an analytic model to show that interaction between frontogenesis and cabbeling is a possible mechanism for mode water formation.

Observationally based estimates of "nonlinear water mass transformation" (NWMT; water mass transformation due to the nonlinearities of the EOS) are harder to obtain, since large uncertainties exist regarding the spatial and temporal variability of the mixing process. Until now, observational estimates have been limited to using a constant eddy diffusion coefficient applied to a "mean year" gridded global climatology [*Klocker and McDougall*, 2010], or alternatively to estimating the globally integrated cabelling necessary to balance the net decrease in density by thermal and haline surface forcing, and as such avoiding the need to specify an eddy diffusion coefficient [*Schanze and Schmitt*, 2013].

Recently much progress has been made on our understanding and quantification of the spatial variability of eddy diffusion coefficients used to parameterize the effect of mixing by mesoscale eddies [*Zhurbas and Oh*, 2004; *Rypina et al.*, 2012; *Abernathey and Marshall*, 2013; *Klocker and Abernathey*, 2013; *Tulloch et al.*, 2014; *Cole et al.*, 2015]. In addition, the availability of ARGO data has significantly improved the representation of the mean ocean state in gridded climatologies. In this study we make use of this recent progress and use the latest available climatologies and estimates of eddy diffusivities to revisit the role of cabbeling and thermobaricity for global WMT budgets. We show that these spatially varying estimates of eddy diffusivities have a large impact on the production of Antarctic Intermediate Water (AAIW).

2. The Water Mass Transformation Framework

Here an expression for water mass transformation (WMT) is derived which allows for the separation of the contributions by surface fluxes, horizontal mixing, vertical mixing, cabbeling and thermobaricity.

The amount of mixing in the ocean is dictated by stirring processes, such as that by mesoscale eddies or breaking internal waves [*Garrett*, 2001]. In the ocean interior, mesoscale eddies stir tracers along isopycnals, and their mixing is subsequently parameterised as *isopycnal* down-gradient diffusion using an eddy diffusion coefficient K operating on isopycnal tracer gradients, with the tracer flux given by $K\nabla_N C$ [*Redi*, 1982; *Griffies*, 1998; *McDougall et al.*, 2014], where C is a tracer that is independent of pressure for an adiabatic and isohaline movement [e.g., Θ and S_A, *IOC et al.*, 2010, Appendix A9 and B]. Near the surface, mesoscale fluxes are geometrically constrained to be horizontal and consequently acquire a diapycnal component [*Treguier et al.*, 1997; *Ferrari et al.*, 2008]. This is often described as "surface diabatic mixing" [*Tandon and Garrett*, 1997] and is parameterized as *horizontal* down-gradient diffusion using an eddy diffusion coefficient K operating on horizontal tracer gradients, with the tracer flux given by $K\nabla_H C$, where ∇_H is the horizontal gradient. Small-scale isotropic down-gradient turbulent diffusion with diffusion coefficient D, representing small scale turbulent stirring events such as breaking internal waves, produces a vertical tracer flux $D\partial C/\partial z$. The isotropic nature of the direction of small-scale diffusion is discussed in *McDougall et al.* [2014]; this mixing can, to a good approximation, be considered vertical. The focus of this study is on the role of mesoscale mixing; however, we provide basic estimates of all components, including vertical mixing, for comparison.

The tendency of C due to mixing processes is then estimated by:

$$d_C = \underbrace{\nabla_H \cdot (K \nabla_H C)}_{d_C^{\mathrm{hor}}} + \underbrace{\frac{\partial \gamma^{\mathrm{n}}}{\partial z} \nabla_N \cdot \left(\left(\frac{\partial \gamma^{\mathrm{n}}}{\partial z} \right)^{-1} K \nabla_N C \right)}_{d_C^{\mathrm{iso}}} + \underbrace{\frac{\partial}{\partial z} \left(D \frac{\partial C}{\partial z} \right)}_{d_C^{\mathrm{ver}}}, \tag{1}$$

where d_C^{iso} operates in the ocean interior (i.e. below the mixed layer) on isopycnal tracer gradients and d_C^{hor} operates in the mixed layer on horizontal tracer gradients. The term d_C^{iso} contains the thickness flux of Neutral Density (γ^{n}, detailed below). By replacing tracer C with S_{A} and Θ, the diffusion of salt and heat is obtained, respectively.

In the ocean, fluid parcels move in directions along which they do not encounter buoyant forces. These directions define the local neutral tangent plane [*McDougall*, 1987b]. Because of the nonlinearities in the equation of state, these neutral tangent planes cannot be connected globally to form a well-defined surface in three-dimensional space (e.g. *McDougall*, 1987b; *Klocker and McDougall*, 2010). Nevertheless, it is possible to minimize the difference between neutral tangent planes and an isopycnal surface, minimizing fictious diapycnal mixing known as the "Veronis effect" [*Veronis*, 1975; *Klocker et al.*, 2009], by using Neutral Density (γ^{n}) as defined by *Jackett and McDougall* [1997]:

$$\nabla \gamma^{\mathrm{n}} \approx b \left(\nabla \rho - \rho \kappa \nabla P \right) = b \rho \left(-\alpha \nabla \Theta + \beta \nabla S_{\mathrm{A}} \right). \tag{2}$$

Here α and β are the thermal and haline expansion coefficients, respectively, ρ is the *in-situ* density, and $b = |\nabla \gamma^{\mathrm{n}}| / |\nabla \rho_r|$ [*Iudicone et al.*, 2008a] is an integrating factor that allows for the construction of a Neutral Density surface from non-connecting tangents of locally referenced potential density ρ_r, referenced to local mean pressure at this general location [*McDougall and Jackett*, 1988]. *Iudicone et al.* [2008a] showed in their Appendix A [using *McDougall and Jackett*, 2005] that the material derivative of γ^{n} is well approxi-

mated by the expression,

$$\frac{D\gamma^{\mathrm{n}}}{Dt} \approx\ b\gamma^{\mathrm{n}}\left(-\alpha\frac{D\Theta}{Dt}+\beta\frac{DS_{\mathrm{A}}}{Dt}\right), \tag{3}$$

where α and β are evaluated at the local pressure.

The material derivative of Θ ($D\Theta/Dt$) represents the rate of change in Θ due to the convergence of boundary heat fluxes ($f_\Theta = Q/(\rho_r C_p^0)$, in [K m s^{-1}]) and diffusive Θ fluxes d_Θ. Here Q is a surface heat flux (Wm^{-2}), and C_p^0 is the heat capacity (J kg^{-1} K^{-1}). Similarly the diffusive S_{A} fluxes $d_{S_{\mathrm{A}}}$ and the boundary salt fluxes ($f_{S_{\mathrm{A}}} = S_{\mathrm{A}}(E-P-R)$, in [$S_{\mathrm{A}}$ m s^{-1}]) are defined, such that $f_{\gamma^{\mathrm{n}}} = b\gamma^{\mathrm{n}}\left(-\alpha\nabla f_\Theta + \beta\nabla f_{S_{\mathrm{A}}}\right)$.

The effects of geothermal heating, solar penetration of heat, and sea-ice interactions can be included in the boundary forcing terms. By inserting Eq. (1) in Eq. (3), an expression for the material derivative of γ^{n} is given by:

$$\frac{D\gamma^{\mathrm{n}}}{Dt} \approx\ b\gamma^{\mathrm{n}}\left(-\alpha d_\Theta^{\mathrm{ver}}+\beta d_{S_{\mathrm{A}}}^{\mathrm{ver}}-\alpha d_\Theta^{\mathrm{hor}}+\beta d_{S_{\mathrm{A}}}^{\mathrm{hor}}\right)+b\gamma^{\mathrm{n}}\left(-\alpha d_\Theta^{\mathrm{iso}}+\beta d_{S_{\mathrm{A}}}^{\mathrm{iso}}\right)+f_{\gamma^{\mathrm{n}}}, \tag{4}$$

Using the fact that along a Neutral Density surface the density gradients due to S_{A} and Θ gradients are exactly compensated, leading to $\alpha\nabla_N\Theta = \beta\nabla_N S_{\mathrm{A}}$, isopycnal diffusion is rewritten into a contribution from cabbeling (C_{b}) and thermobaricity (T_{b}):

$$\left(-\alpha d_\Theta^{\mathrm{iso}}+\beta d_{S_{\mathrm{A}}}^{\mathrm{iso}}\right) = \underbrace{-Kb\gamma^{\mathrm{n}}C_{\mathrm{b}}\left|\nabla_N\Theta\right|^2}_{d_{C_{\mathrm{b}}}}\underbrace{-Kb\gamma^{\mathrm{n}}T_{\mathrm{b}}\nabla_N P\cdot\nabla_N\Theta}_{d_{T_{\mathrm{b}}}}. \tag{5}$$

Here C_{b} and T_{b} are the cabbeling and thermobaricity coefficients as defined by *McDougall* [1984, 1987b] and *Klocker and McDougall* [2010], leaving:

$$\frac{D\gamma^{\mathrm{n}}}{Dt} \approx\ b\gamma^{\mathrm{n}}\left(-\alpha d_\Theta^{\mathrm{ver}}+\beta d_{S_{\mathrm{A}}}^{\mathrm{ver}}-\alpha d_\Theta^{\mathrm{hor}}+\beta d_{S_{\mathrm{A}}}^{\mathrm{hor}}\right)+f_{\gamma^{\mathrm{n}}}+d_{C_{\mathrm{b}}}+d_{T_{\mathrm{b}}}. \tag{6}$$

Eqs. (5) and (6) are used to separately calculate the contribution from both cabbeling and thermobaricity to WMT. Eq. (6) provides the local tendency in γ^{n} (in kg m^{-3} s^{-1}).

The total WMT (in Sv, where 1 Sv = 10^6 m^3 s^{-1}) is given by the integral:

$$\begin{aligned} T_{\gamma^{\mathrm{n}}}(\gamma^{\mathrm{n}}) &= -\frac{\partial}{\partial \gamma^{\mathrm{n}}} \int_{V(\gamma^{\mathrm{n}} hat \leq \gamma^{\mathrm{n}})} \frac{D\gamma^{\mathrm{n}}}{Dt} dV, \\ &= M^{\mathrm{ver}}(\gamma^{\mathrm{n}}) + M^{\mathrm{hor}}(\gamma^{\mathrm{n}}) + F(\gamma^{\mathrm{n}}) + M^{C_{\mathrm{b}}}(\gamma^{\mathrm{n}}) + M^{T_{\mathrm{b}}}(\gamma^{\mathrm{n}}). \end{aligned} \tag{7}$$

Here $\int_{V(\hat{\gamma}^{\mathrm{n}} \leq \gamma^{\mathrm{n}})} dV$ is the integral over the volume for which $\hat{\gamma}^{\mathrm{n}} \leq \gamma^{\mathrm{n}}$. M^{ver}, M^{hor}, F, $M^{C_{\mathrm{b}}}$ and $M^{T_{\mathrm{b}}}$ are the WMT rates as a result of vertical mixing, horizontal mixing, surface buoyancy forcing, cabbeling and thermobaricity, respectively, as a function of γ^{n}. The nonlinear water mass transformation (NWMT) is defined as the sum of cabbeling and thermobaricity, i.e. $N_{\mathrm{L}} = M^{C_{\mathrm{b}}} + M^{T_{\mathrm{b}}}$. The numerical implementation of Eq. (7) is discussed in Appendix A, together with a method to provide spatial maps of transformation [e.g. *Maze et al.*, 2009]. The calculation of isopycnal tracer gradients ($\nabla_N C$) is non-trivial and is explained in Appendix B. Finally, the total formation rate of water of a particular density range is given by is given by,

$$F_{\gamma^{\mathrm{n}}}(\gamma^{\mathrm{n}}) = \int_{\gamma_1^{\mathrm{n}}}^{\gamma_2^{\mathrm{n}}} -\frac{\partial T_{\gamma^{\mathrm{n}}}(\gamma^{\mathrm{n}})}{\partial \gamma^{\mathrm{n}}} d\gamma^{\mathrm{n}} = T_{\gamma^{\mathrm{n}}}(\gamma_1^{\mathrm{n}}) - T_{\gamma^{\mathrm{n}}}(\gamma_2^{\mathrm{n}}). \tag{8}$$

3. Hydrographic and Diffusivity Data

Here we describe the different data products used as inputs for our study. For the observationally based climatology, we employ the World Ocean Atlas 2013 (version 2), which is a set of objectively analyzed (1° grid) climatological fields of temperature, salinity, and other tracers at standard depth levels for annual, seasonal, and monthly compositing periods for the world ocean [*Boyer et al.*, 2013]. Monthly means for the upper 1500 m are used, while it is assumed that the deep ocean has little seasonal variation, such that seasonal means (repeated per quarter) are used for the interior (below 1500 m).

TEOS-10 software [*IOC et al.*, 2010; *McDougall and Barker*, 2011] is applied to convert the data to S_A and Θ and calculate the mixed layer depth for each month (based on *de Boyer Montégut et al.* [2004]). As static stability is required for the calculation of isopycnal surfaces, the data is stabilized ($N^2 > 0$ everywhere) using a minimal adjustment of S_A and Θ, within the measurement error [*Jackett and McDougall*, 1995].

Surface boundary fluxes are taken from the product of *Yeager and Large* [2008]. In this product, the global air-sea heat and water flux components are computed by applying bulk formulae to an atmosphere and ocean state. The atmospheric state is from version 2 of CORE (Common Ocean Reference Experiment) atmospheric state fields from 1949 to 2006, which derive from multiple input sources [*Large and Yeager*, 2009]. The ocean state is from the Hadley OI-SST product at monthly resolution. The *Yeager and Large* [2008] product has a spatial resolution of 1^o x 1^o grid spacing and is converted to a "standard year" by averaging surface fluxes for each calendar month. We recognize that many other air-sea flux datasets exist which may produce slightly different results–the goal here is simply to provide a point of comparison for the NWMT.

The Neutral Density software of *Jackett and McDougall* [1997] is used to calculate γ^n. The b factor in this study has an average of $b \approx 1.1$ (including spikes of $b > 10000$), showing that the use of Neutral Density is well justified in this data set. Data points for which $b > 5$ (about 1.5 % of data) are discarded, while $2 < b < 5$ are replaced by $b = 2$ (about 6.5 % of data). Due to the specific fitting region applied in the Neutral Density software, the northward extent is limited to 70°N. Vertical profiles of γ^n are stabilized in the following way: if $\gamma^n(z_{k+1}) < \gamma^n(z_k)$, then $\gamma^n_{\text{stable}}(z_{k+1}) = \gamma^n(z_k) + \epsilon_{\gamma^n}$, where $\epsilon_{\gamma^n} = 1$

x 10^{-5} and z_{k+1} is deeper than z_k. This process is iteratively repeated until all vertical profiles are stable and leads to very small differences.

Cabbeling, thermobaricity and horizontal mixing strongly depend on the spatial structure of the eddy diffusivity K. To understand this sensitivity, we employ two different choices of K. Results are first obtained using a constant value of $K = 1000$ m^2 s^{-1}. For a more realistic calculation, we then use the recent estimate of K from *Cole et al.* [2015], who used salinity variance from ARGO profiles to resolve the three-dimensional structure of isopycnal mixing (Fig. 1). For depths greater than $H_{\max}$, the depth of the deepest K estimate of each vertical profile, we extrapolate vertically using $K(x, y, z < -H_{\max}(x, y)) = K_0(x, y)\exp\left(-\left(z + H_{\max}\right)\ln(0.25)/h_{\text{decay}}\right)$, using a 75% decay over $h_{\text{decay}} = 1500$ m as obtained from the vertical structure of the horizontal average of the raw global data, and $K_0(x, y)$ is K given at $H_{\max}(x, y)$. The height z is positive upward. Missing values in the mixed-layer and for high latitudes (beyond the reach of the data-set), are calculated using a nearest neighbor extrapolation. A $K_{\max} = 2.5 \times 10^4$ m^2 s^{-1} is applied. Near the surface, the estimate from *Cole et al.* [2015] is comparable to estimates obtained from satellite data [*Abernathey and Marshall*, 2013; *Klocker and Abernathey*, 2013].

Due to the limitations of the K-estimates and Neutral Density software, the Arctic and marginal seas such as the Mediterranean, are excluded from our calculations (see dark blue shading Fig. 1).

To calculate the effects of small scale turbulent mixing requires an estimate or parameterisation for the spatial variations of turbulent diffusivity D, as for example given

by *Bryan and Lewis* [1979]; *St. Laurent et al.* [2002]; *Nycander* [2005]; *Polzin* [2009]; *Nikurashin and Ferrari* [2011] and *Waterhouse et al.* [2014]. The focus of this study is on cabbeling and thermobaricity, which do not depend on D. However, we provide a crude estimate for the sake of comparison by employing a simple constant value of $D = 3 \times 10^{-5}$ m^2 s^{-1}. The consequence of spatially variable D for WMT is a topic of ongoing research [e.g. *Mashayek et al.*, 2015; *Ferrari et al.*, 2016].

4. Results

Here an interpretation of the results is provided, using constant (scenario 1) and spatially varying (scenario 2) eddy diffusivities. Note that, for a steady-state ocean, the total water mass transformation (WMT) at every γ^n would be zero. However, the climatology is an averaged representation of data unequally distributed in space and time, leading to inaccuracies in the representation of the ocean's state. In addition, the air-sea heat and freshwater fluxes are imperfect as they do not include the effects of sea-ice interaction, geothermal heating and solar penetration depth. We also do not know the exact spatial and temporal distribution of the small-scale and mesoscale diffusivities. Therefore, this study does not attempt to close the WMT budget, but instead focuses on quantifying the WMT due to cabbeling and thermobaricity, and understanding the influence of introducing a spatially varying mesoscale diffusivity.

The WMT by surface fluxes (yellow line, Fig. 2) is practically identical to Fig. 6a of *Iudicone et al.* [2008a], providing a good reference to contrast the other terms against. Considering the use of a constant $D = 3 \times 10^{-5}$ m^2 s^{-1}, the WMT by small-scale mixing

(red line, Fig. 2) is a rough estimate, against which we can compare the nonlinear WMT (NWMT, $N_{\mathrm{L}} = M^{C_{\mathrm{b}}} + M^{T_{\mathrm{b}}}$).

Surface forcing causes water-mass divergence by transforming light water into lighter water and dense water into denser water, while mixing (red and green lines, Fig. 2) has an opposite structure, driving convergence (i.e. homogenization). Comparing horizontal mixing for both scenarios (dashed and solid red lines, Fig. 2) shows that the WMT by horizontal mixing has similar shape for both scenarios but a larger magnitude for varying K (scenario 2). This shows that K is enhanced where horizontal Θ and S_{A} gradients are already large. The total NWMT for both scenarios (dashed and solid blue lines, Fig. 2) play a significant role in the total WMT budget for $\gamma^{\mathrm{n}} > 26$ kg m^{-3} and leads to additional densification.

4.1. Water mass transformation by Cabbeling and Thermobaricity

Here the NWMT for $\gamma^{\mathrm{n}} > 24.5$ kg m^{-3} is split up into its cabbeling ($M^{C_{\mathrm{b}}}$) and thermobaricity ($M^{T_{\mathrm{b}}}$) components, from which it is evident that there are large differences between both scenarios (Fig. 3a). NWMT by $M^{C_{\mathrm{b}}}$ and $M^{T_{\mathrm{b}}}$, using a constant eddy diffusivity (scenario 1) are comparable in distribution to that shown in Fig. 3b of *Klocker and McDougall* [2010], which is based on the WOCE climatology with the same constant eddy diffusivity of $K = 1000$ m^2 s^{-1}. The magnitude of the NWMT is larger for this study. Although WOA13 has lower spatial resolution (1° Vs 0.5° grid) than WOCE, it includes more data and has a higher temporal resolution (monthly vs. yearly), allowing for sharper fronts and therefore larger gradients.

When comparing the differences between both scenarios, the choice of $K = 1000$ m^2 s^{-1} is rather arbitrary, such that the difference in distribution, and not the magnitude, is of most interest. For scenario 2 (varying K), WMT by M^{C_b} shows peaks of 21 Sv at $\gamma^\mathrm{n} \approx 27.25$ kg m^{-3} and 25 Sv at $\gamma^\mathrm{n} \approx 28.1$ kg m^{-3} (Fig. 3a), while scenario 1 (constant K) only shows the second peak and is about 21 Sv. This shows that the first peak is due to enhanced eddy diffusivities, while the second peak is mostly the result of relatively strong tracer gradients within that γ^n range.

We now further examine scenario 2, splitting M^{C_b} and M^{T_b} into contributions from the different ocean basins (Fig. 3b). This reveals that the second peak at $\gamma^\mathrm{n} \approx 28.1$ kg m^{-3} leads to 15 Sv of dense Lower Circumpolar Deep Water (LCDW) formation, out of Upper Circumpolar Deep Water (UCDW) and light LCDW. It is also seen that M^{C_b} and M^{T_b} contribute to 10 Sv of AABW formation through transformation of dense LCDW. These processes take place near the Antarctic continental shelves (Figs. 3 and 4b,d). However, these values need to be interpreted with caution; hydrographic data are sparse in this region, and the K estimate *Cole et al.* [2015] does not reach these latitudes or depth and here is produced by extrapolation.

The WMT peak for cabbeling at $\gamma^\mathrm{n} \approx 27.25$ kg m^{-3} is due to WMT in the Indo-Pacific (3 Sv), Atlantic (5 Sv) and Southern Ocean (12 Sv, Fig. 3b). Using Eq. (8) we find that for the AAIW range, there is formation of 4.1 Sv by Cabbeling, 29 Sv by horizontal mixing, -29 by vertical mixing and -26 Sv by surface forcing (Figs. 3a and 4a). For dense AAIW ($27.25 \leq \gamma^\mathrm{n} \leq 27.5$ kg m^{-3}) there is formation of 8.7 Sv by Cabbeling, 11.9 Sv by horizontal mixing, -2.9 by vertical mixing and -41.2 Sv by surface forcing. Note

that especially the formation by surface forcing and vertical mixing are bulk estimates. However, most of the formation by surface forcing is compensated by that of horizontal mixing processes in the mixed layer, as also found by *Iudicone et al.* [2008b], such that the effect of cabbeling remains important.

In the Atlantic, we can conclude that cabbeling is significant in the Gulf Stream area (Fig. 4a). The cabbeling peaks for the AAIW-range and LCDW-range of 15 Sv and 25 Sv, respectively, are larger than the peaks of 6 Sv and 8 Sv found by *Urakawa and Hasumi* [2012] for an eddy-permitting numerical model using σ_2 (their Fig. 5c). The second peak is due to transformation of LCDW and AABW in the Southern Ocean (Fig 3).

M^{T_b} is mostly important in the Southern Ocean for $\gamma^\mathrm{n} \approx 27.25 - 28.25$ kg m^{-3} and generally smaller than that by M^{C_b} (Fig. 3). M^{T_b} is spatially variable in sign and magnitude and integrated over a neutral surface, generally positive, with the exception of the AABW range (Fig. 3). M^{T_b} contributes to about 7 Sv of LCDW formation and shows some signs that it may lead to lightening (upwelling) of AABW.

5. Discussion and Conclusions

WMT by cabbeling and thermobaricity is calculated in a Neutral Density γ^n framework. The results are obtained by combining an observationally based gridded climatology with two scenarios of eddy diffusivities: a constant value of $K = 1000$ m^2 s^{-1}, and the spatially variable, observationally based estimates of K from *Cole et al.* [2015].

When using spatially varying K, a new WMT peak is observed due to cabbeling, for $\gamma^\mathrm{n} \approx 27.25$ kg m^{-3}, allowing for about 8.7 Sv of AAIW formation in the Southern Ocean. This supports the conclusion of *Nycander et al.* [2015], who showed that cabbeling is

essential for the formation of AAIW in a numerical ocean model. While *Nycander et al.* [2015] used an ocean model with constant K, our results suggest that, in the real ocean, intense mixing on the flanks of the Antarctic Circumpolar Current [*Abernathey et al.*, 2010] is part of the AAIW formation process.

One hypothesized mechanism of AAIW formation is through transformation of upwelled CDW and SAMW at the surface, in combination with wind driven subduction [*Sloyan and Rintoul*, 2001; *Hanawa and Talley*, 2001]. At the same time, part of the transformation by surface buoyancy fluxes is directly compensated by horizontal mixing, and there is evidence to suggest that in much of the region where AAIW is formed, there is in fact wind driven upwelling rather than downwelling [*Sallée et al.*, 2010]. Hence, AAIW formation is not yet a fully understood process. Here an additional AAIW formation mechanism is proposed.

Parallel to the results of *Nycander et al.* [2015], *Saenko and Weaver* [2001] found that wind-driven sea ice motion is essential for the formation of AAIW in a numerical ocean model. In relation to this, *Abernathey et al.* [2016] showed that northward transport of sea ice from Antarctica leads to a significant freshwater flux as a result of melting. *Stewart and Haine* [2016] showed that the AAIW region is mostly a 'beta' ocean, indicating that stratification of S_A is important for the local dynamics. Based on these previous studies and the results presented here, the following mechanism is proposed to be a significant contribution to dense AAIW formation. In the Southern Ocean, the melting of northward-advected sea ice leads to a fresh and cold surface layer, contrasting the relatively salty and warm ambient water. This produces strong isopycnal Θ and S_A gradients (cold and

fresh to warm and salty) that are ideal for cabbeling in an area where the dynamics of the Antarctic Circumpolar Current allows for enhanced mesoscale mixing processes. The combined effect of these processes then leads to formation of AAIW.

This study also indicates that formation of LCDW, NADW and AABW is influenced by both cabbeling and thermobaricity. Although this provides a good hint of what is happening, these results are influenced by data sparseness and a less accurate representation of K, and therefore require further study.

To obtain the correct WMT rates by cabbeling and thermobaricity, especially for the formation of AAIW, a correct implementation of spatially varying eddy diffusivity coefficients appears to be essential. AAIW plays a key role in the Earth system's heat, nutrient, and carbon budgets [*Hanawa and Talley*, 2001; *Sarmiento et al.*, 2004; *Iudicone et al.*, 2011], and hence it is crucial to understand its formation mechanism and its likely change in a future climate. This study represents an advance in our knowledge of WMT thanks to improved estimates of eddy diffusivities. Further refining such estimates will therefore lead to an improved understanding of our climate system.

Appendix A: Nummerical implementation and transformation maps

Here the numerical implementation of Eq. (7) is discussed, and subsequently the calculation of a mappable diapycnal velocity. A tracer is defined at the a T-grid at gridpoint (x_i, y_j, z_k, t_τ). Here $i = 1, 2, ..., I$, where I is the total number of longitude location in the ocean. In a similar way j and J represent latitude, k and K represent depth and τ and T represent time. The tracer is given on $\Theta_{ijk\tau} = \Theta(x_i, y_j, z_k, t_\tau)$. This location represents a volume $\Delta V_{ijk} = dx_i dy_j dz_k$. Cabbeling at a T-grid is given

by $M^{C_\mathrm{b}}_{ijk\tau} = -K_{ijk\tau} b_{ijk\tau} \gamma^\mathrm{n}_{ijk\tau} c_{\mathrm{b},ijk\tau} \left|\nabla_N \Theta_{ijk\tau}\right|^2$, giving:

$$T^\mathrm{ntr}(\gamma^\mathrm{n}) = -\frac{1}{T}\sum_{\tau=1}^{T}\sum_{i=1}^{I}\sum_{j=1}^{J}\left[\frac{1}{\Delta\gamma^\mathrm{n}}\sum_{i=k}^{K}\Delta V_{ijk\tau} M^{C_\mathrm{b}}_{ijk\tau} H(\gamma^\mathrm{n}_{ijk\tau}, \gamma^\mathrm{n}, \Delta\gamma^\mathrm{n})\right]. \tag{A1}$$

Here H is the numerical δ-function:

$$H(\gamma^\mathrm{n}_{ijk\tau}, \gamma^\mathrm{n}, \Delta\gamma^\mathrm{n}) = \begin{cases} 1 \text{ if } \left(\gamma^\mathrm{n} - \frac{1}{2}\Delta\gamma^\mathrm{n}\right) < \gamma^\mathrm{n}_{ijk\tau} \leq \left(\gamma^\mathrm{n} + \frac{1}{2}\Delta\gamma^\mathrm{n}\right) \\ 0 \text{ if otherwise} \end{cases}, \tag{A2}$$

Applying $H(\gamma^\mathrm{n}_{ijk\tau}, \gamma^\mathrm{n}, \Delta\gamma^\mathrm{n})$ is the same as taking the derivative with respect to γ^n. Note C_b can be replaced with other transformation processes. The component within brackets in Eq. (A1) can be represented as a spatial map of transformation per area (Sv m^{-2}), which is equivalent to a diapycnal velocity (m s^{-1}). For this, the transformation at each location is divided by the horizontal area $\Delta A_{ij} = dx_i dy_j$ (which is a very accurate approximation of the isopycnal surface area) leaving:

$$e_{ij\tau}(\gamma^\mathrm{n}) = -\left[1/\gamma^\mathrm{n}\sum_{i=k}^{K}\Delta V_{ijk\tau} M^{C_\mathrm{b}}_{ijk\tau} H(\gamma^\mathrm{n}_{ijk\tau}, \gamma^\mathrm{n}, \Delta\gamma^\mathrm{n})\right]/\Delta A_{ij}. \tag{A3}$$

For a particular γ^n and time, a map of the diapycnal velocity $e_{ij\tau}(\gamma^\mathrm{n})$ can be obtained.

Appendix B: Calculating isopycnal tracer gradients

To calculate isopycnal Θ gradients $\nabla_N\Theta$, the Redi diffusion tensor [*Redi*, 1982] can be used in combination with the small slope approximation [*Gent and McWilliams*, 1990], as given in Eq. (13) of [*McDougall et al.*, 2014]. For example, the isopycnal Θ gradient in the x-direction, along a Neutral Density surface, is given by $\partial\Theta/\partial x + s_x \partial\Theta/\partial z$, where $s_x = -(\partial\gamma^\mathrm{n}/\partial x)/(\partial\gamma^\mathrm{n}/\partial z)$. As this requires dividing $(\partial\gamma^\mathrm{n}/\partial z)$, which can be nearly zero, leading to spikes or a general overestimation of the slope and therefore $\nabla_N\Theta$.

To avoid singularity, we calculate the slope as $s_x = \Delta z/\Delta x$, such that:

$$\nabla_N\Theta\cdot\mathbf{e_1} \approx \frac{\Delta\Theta|_{\gamma^\mathrm{n}}}{\Delta x} = \frac{\partial\Theta}{\partial x} + s_x\frac{\partial\Theta}{\partial z} \tag{A4}$$

Here $\Delta\Theta|_{\gamma^n}$ means the 'difference in Θ at constant γ'. The same applies for the y direction, such that the isopycnal Θ gradient is given by

$$\nabla_N\Theta \approx \left(\frac{\Delta\Theta|_{\gamma^n}}{\Delta x}, \frac{\Delta\Theta|_{\gamma^n}}{\Delta y}, s_x\frac{\Delta\Theta|_{\gamma^n}}{\Delta x} + s_y\frac{\Delta\Theta|_{\gamma^n}}{\Delta y}\right) . \tag{A5}$$

The values for Δx, Δy, Δz are obtained through an interpolation method. Consider only longitude and depth, such that γ^n is given at the T-grid as $\gamma^n_{i,k} = \gamma^n(x_i, z_k)$. Use averaging to obtain the values at $\gamma^n_{i+0.5,k} = \gamma^n(x_{i+0.5}, z_k)$, which is at the edges of the T-grid. Start with $\gamma^n_{i+0.5,\kappa}$, where κ is a fixed depth. Using linear interpolation, $\gamma^n_{i+1.5,k}$ is obtained for the depth $z_{\rm int}$, on profile $x_{i+1.5}$, for which $\gamma^n_{i+0.5,\kappa} = \gamma^n_{i+1.5,z_{\rm int}}$. A γ^n surface has now been constructed, from profile $x_{i+0.5}$ to profile $x_{i+1.5}$, such that $\Delta x = (x_{i+1.5} - x_{i+0.5})$ and $\Delta z = (z_\kappa - z_{\rm int})$. In a similar way we can calculate $\Delta\Theta|_\gamma/\Delta y$ and use both results to calculate the gradient in the z-direction as in Eq. (A5). The slopes are given at the mid-depth $z_m = 0.5(z_{i+0.5,\kappa} + z_{\rm int})$, at the mid point between the two profiles x_{i+1}. After repeating this for each i,j and k, linear interpolation is used to provide the values of the slopes back on the original T-grid depths $x_{i,k}$. The same procedure is applied to obtain $\nabla_N S_A$ and $\nabla_N P$. If $z_{\rm int}$ is interpolated through the ocean surface or bottom, the slopes are not calculated.

Acknowledgments. SG and RPA acknowledge support by the NASA Grant NNX14AI46G. AK was supported by an Australian Research Council Discovery Early Career Researcher Award (DE140100076). We thank Trevor McDougall for useful discussion on this work. We thank Paul Barker for providing a preliminary version of the new gsw-based stabilization method and helping to get the Neutral Density code to work

together with Jonathan Sattelberger. We thank Sylvia Cole and Cimarron Wortham for providing the mesoscale diffusivities.

References

Abernathey, R., J. Marshall, M. Mazloff, and E. Shuckburgh (2010), Enhancement of mesoscale eddy stirring at steering levels in the southern ocean, *Journal of Physical Oceanography*, *40*(1), 170–184, doi:10.1175/2009JPO4201.1.

Abernathey, R. P., and J. Marshall (2013), Global surface eddy diffusivities derived from satellite altimetry, *Journal of Geophysical Research: Oceans*, *118*(2), 901–916, doi:10.1002/jgrc.20066.

Abernathey, R. P., I. Cerovecki, P. R. Holland, E. Newsom, M. Mazloff, and L. D. Talley (2016), Water-mass transformation by sea ice in the upper branch of the southern ocean overturning, *Nature Geosci*, *9*, 596–601, doi:10.1038/ngeo2749.

Boyer, T., J. I. Antonov, O. K. Baranova, C. Coleman, H. E. Garcia, A. Grodsky, D. R. Johnson, R. A. Locarnini, A. V. Mishonov, T. O'Brien, C. Paver, J. Reagan, D. Seidov, I. V. Smolyar, and M. M. Zweng (2013), World ocean database 2013, noaa atlas nesdis 72, *http://doi.org/10.7289/V5NZ85MT*, 209 pp.

Bryan, K., and L. J. Lewis (1979), A water mass model of the World Ocean, *Journal of Geophysical Research: Oceans*, *84*(C5), 2503–2517, doi:10.1029/JC084iC05p02503.

Cole, S. T., C. Wortham, E. Kunze, and W. B. Owens (2015), Eddy stirring and horizontal diffusivity from argo float observations: Geographic and depth variability, *Geophysical Research Letters*, *42*(10), 3989–3997, doi:10.1002/2015GL063827, 2015GL063827.

de Boyer Montégut, C., G. Madec, A. S. Fischer, A. Lazar, and D. Iudicone (2004), Mixed layer depth over the global ocean: An examination of profile data and a profile-based climatology, *Journal of Geophysical Research: Oceans*, *109*(C12), n/a–n/a, doi: 10.1029/2004JC002378, c12003.

Ferrari, R., J. C. McWilliams, V. M. Canuto, and M. Dubovikov (2008), Parameterization of eddy fluxes near oceanic boundaries, *Journal of Climate*, *21*(12), 2770–2789, doi: 10.1175/2007JCLI1510.1.

Ferrari, R., A. Mashayek, T. J. McDougall, M. Nikurashin, and J.-M. Campin (2016), Turning ocean mixing upside down, *Journal of Physical Oceanography*, *46*(7), 2239–2261.

Garrett, C. (2001), Stirring and mixing: What are the rate-controlling processes?, in *Proceedings of the Twelfth 'Aha Huliko'a Hawaiian Winter Workshop*, pp. 1–8.

Gent, P. R., and J. C. McWilliams (1990), Isopycnal Mixing in Ocean Circulation Models., *Journal of Physical Oceanography*, *20*(1), 150–155, doi:10.1175/1520-0485(1990)020<0150:IMIOCM>2.0.CO;2.

Griffies, S. M. (1998), The Gent–McWilliams Skew Flux., *Journal of Physical Oceanography*, *28*(5), 831–841, doi:10.1175/1520-0485(1998)028¡0831:TGMSF¿2.0.CO;2.

Hanawa, K., and L. D. Talley (2001), *Ocean Circulation and Climate.*, chap. Mode Waters, pp. 373–386, International Geophysics Series, Academic Press.

Hieronymus, M. (2014), A note on the influence of spatially varying diffusivities on the evolution of buoyancy with a nonlinear equation of state, *Journal of Physical Oceanography*, *44*(12), 3255–3261, doi:10.1175/JPO-D-13-0262.1.

IOC, SCOR, and IAPSO (2010), *The international thermodynamic equation of seawater – 2010: Calculation and use of thermodynamic properties.*, Intergovernmental Oceanographic Commission, Manuals and Guides. UNESCO (English), [Available online at www.TEOS-10.org].

Iudicone, D., G. Madec, and T. J. McDougall (2008a), Water-Mass Transformations in a Neutral Density Framework and the Key Role of Light Penetration., *Journal of Physical Oceanography*, *38*(7), 1357–1376, doi:10.1175/2007JPO3464.1.

Iudicone, D., G. Madec, B. Blanke, and S. Speich (2008b), The role of southern ocean surface forcings and mixing in the global conveyor, *Journal of Physical Oceanography*, *38*(7), 1377–1400, doi:10.1175/2008JPO3519.1.

Iudicone, D., K. B. Rodgers, I. Stendardo, O. Aumont, G. Madec, L. Bopp, O. Mangoni, and M. Ribera d'Alcala' (2011), Water masses as a unifying framework for understanding the southern ocean carbon cycle, *Biogeosciences*, *8*(5), 1031–1052, doi:10.5194/bg-8-1031-2011.

Jackett, D. R., and T. J. McDougall (1995), Minimal Adjustment of Hydrographic Profiles to Achieve Static Stability., *Journal of Atmospheric and Oceanic Technology*, *12*(2), 381–389, doi:10.1175/1520-0426(1995)012¡0381:MAOHPT¿2.0.CO;2.

Jackett, D. R., and T. J. McDougall (1997), A Neutral Density Variable for the World's Oceans., *Journal of Physical Oceanography*, *27*(2), 237–263, doi:10.1175/1520-0485(1997)027¡0237:ANDVFT¿2.0.CO;2.

Klocker, A., and R. Abernathey (2013), Global Patterns of Mesoscale Eddy Properties and Diffusivities., *Journal of Physical Oceanography*, *44*(3), 1030–1046, doi:10.1175/JPO-

D-13-0159.1.

Klocker, A., and T. J. McDougall (2010), Influence of the nonlinear equation of state on global estimates of dianeutral advection and diffusion, *Journal of Physical Oceanography*, *40*(8), 1690–1709, doi:10.1175/2010JPO4303.1.

Klocker, A., T. J. McDougall, and D. R. Jackett (2009), A new method for forming approximately neutral surfaces, *Ocean Science*, *5*(2), 155–172, doi:10.5194/os-5-155-2009.

Large, W. G., and S. G. Yeager (2009), The global climatology of an interannually varying air–sea flux data set, *Clim. Dyn.*, *33*(2-3), 341–364.

Marsh, R. (2000), Cabbeling due to isopycnal mixing in isopycnic coordinate models, *Journal of Physical Oceanography*, *30*(7), 1757–1775, doi:10.1175/1520-0485(2000)030¡1757:CDTIMI¿2.0.CO;2.

Mashayek, A., R. Ferrari, M. Nikurashin, and W. Peltier (2015), Influence of enhanced abyssal diapycnal mixing on stratification and the ocean overturning circulation, *Journal of Physical Oceanography*, *45*(10), 2580–2597.

Maze, G., G. Forget, M. Buckley, J. Marshall, and I. Cerovecki (2009), Using transformation and formation maps to study the role of air–sea heat fluxes in north atlantic eighteen degree water formation, *Journal of Physical Oceanography*, *39*(8), 1818–1835, doi:10.1175/2009JPO3985.1.

McDougall, T., and P. M. Barker (2011), *Getting started with TEOS-10 and the Gibbs Seawater (GSW) Oceanographic Toolbox.*, SCOR/IAPSO, WG127, ISBN 978-0-646-55621-5.

McDougall, T. J. (1984), The Relative Roles of Diapycnal and Isopycnal Mixing on Subsurface Water Mass Conversion., *Journal of Physical Oceanography*, *14*(10), 1577–1589, doi:10.1175/1520-0485(1984)014¡1577:TRRODA¿2.0.CO;2.

McDougall, T. J. (1987a), Thermobaricity, cabbeling, and water-mass conversion., *Journal of Geophysical Research: Oceans*, *92*(C5), 5448–5464, doi:10.1029/JC092iC05p05448.

McDougall, T. J. (1987b), Neutral Surfaces., *Journal of Physical Oceanography*, *17*(11), 1950–1964, doi:10.1175/1520-0485(1987)017¡1950:NS¿2.0.CO;2.

McDougall, T. J. (2003), Potential Enthalpy: A Conservative Oceanic Variable for Evaluating Heat Content and Heat Fluxes., *Journal of Physical Oceanography*, *33*(5), 945–963, doi:10.1175/1520-0485(2003)033¡0945:PEACOV¿2.0.CO;2.

McDougall, T. J., and D. R. Jackett (1988), On the helical nature of neutral trajectories in the ocean., *Progress In Oceanography*, *20*(3), 153 – 183, doi:DOI: 10.1016/0079-6611(88)90001-8.

McDougall, T. J., and D. R. Jackett (2005), The material derivative of neutral density, *Journal of Marine Research*, *63*(1), 159–185.

McDougall, T. J., D. R. Jackett, F. J. Millero, R. Pawlowicz, and P. M. Barker (2012), A global algorithm for estimating Absolute Salinity., *Ocean Science*, *8*(6), 1117–1128.

McDougall, T. J., S. Groeskamp, and S. M. Griffies (2014), On geometrical aspects of interior ocean mixing, *Journal of Physical Oceanography*, *44*(8), 2164–2175, doi:10.1175/JPO-D-13-0270.1.

Nikurashin, M., and R. Ferrari (2011), Global energy conversion rate from geostrophic flows into internal lee waves in the deep ocean., *Geophysical Research Letters*, *38*(8),

L08,610, doi:10.1029/2011GL046576.

Nycander, J. (2005), Generation of internal waves in the deep ocean by tides., *Journal of Geophysical Research: Oceans*, *110*(C10), C10,028, doi:10.1029/2004JC002487.

Nycander, J., M. Hieronymus, and F. Roquet (2015), The nonlinear equation of state of sea water and the global water mass distribution, *Geophysical Research Letters*, *42*(18), 7714–7721, doi:10.1002/2015GL065525.

Polzin, K. L. (2009), An abyssal recipe., *Ocean Modelling*, *30*(4), 298–309, doi: http://dx.doi.org/10.1016/j.ocemod.2009.07.006.

Redi, M. H. (1982), Oceanic Isopycnal Mixing by Coordinate Rotation., *Journal of Physical Oceanography*, *12*(10), 1154–1158, doi:10.1175/1520-0485(1982)012¡1154:OIMBCR¿2.0.CO;2.

Rypina, I. I., I. Kamenkovich, P. Berloff, and L. Pratt (2012), Eddy-induced particle dispersion in the near-surface atlantic, *J. Phys. Oceanogr.*, *42*, 2206–2228.

Saenko, O. A., and A. J. Weaver (2001), Importance of wind-driven sea ice motion for the formation of antarctic intermediate water in a global climate model, *Geophysical Research Letters*, *28*(21), 4147–4150, doi:10.1029/2001GL013632.

Sallée, J.-B., K. Speer, S. Rintoul, and S. Wijffels (2010), Southern ocean thermocline ventilation, *Journal of Physical Oceanography*, *40*(3), 509–529, doi: 10.1175/2009JPO4291.1.

Sarmiento, J. L., N. Gruber, M. A. Brzezinski, and J. P. Dunne (2004), High-latitude controls of thermocline nutrients and low latitude biological productivity, *Nature*, *427*(6969), 56–60.

Schanze, J. J., and R. W. Schmitt (2013), Estimates of cabbeling in the global ocean, *Journal of Physical Oceanography*, *43*(4), 698–705, doi:10.1175/JPO-D-12-0119.1.

Sloyan, B. M., and S. R. Rintoul (2001), Circulation, renewal and modification of Antarctic mode and intermediate water, *Journal of Physical Oceanography*, *31*(4), 1005–1030.

St. Laurent, L. C., H. L. Simmons, and S. R. Jayne (2002), Estimating tidally driven mixing in the deep ocean., *Geophysical Research Letters*, *29*(23), 2106, doi: 10.1029/2002GL015633.

Stewart, K. D., and T. W. N. Haine (2016), Thermobaricity in the transition zones between alpha and beta oceans, *Journal of Physical Oceanography*, *46*(6), 1805–1821, doi:10.1175/JPO-D-16-0017.1.

Tandon, A., and C. Garrett (1997), Water mass formation from thermodynamics: a framework for examining compatibility with dynamics, *WOCE*, p. 34.

Thomas, L. N., and C. J. Shakespeare (2015), A new mechanism for mode water formation involving cabbeling and frontogenetic strain at thermohaline fronts, *Journal of Physical Oceanography*, *45*(9), 2444–2456, doi:10.1175/JPO-D-15-0007.1.

Treguier, A. M., I. Held, and V. Larichev (1997), Parameterization of quasigeostrophic eddies in primitive equation ocean models, *J. Phys. Oceanogr.*, *27*, 567–580.

Tulloch, R., R. Ferrari, O. Jahn, A. Klocker, J. LaCasce, J. R. Ledwell, J. Marshall, M.-J. Messias, K. Speer, and A. Watson (2014), Direct estimate of lateral eddy diffusivity upstream of drake passage, *Journal of Physical Oceanography*, *44*(10), 2593–2616.

Urakawa, L. S., and H. Hasumi (2012), Eddy-resolving model estimate of the cabbeling effect on the water mass transformation in the southern ocean, *Journal of Physical*

Oceanography, *42*(8), 1288–1302, doi:10.1175/JPO-D-11-0173.1.

Veronis, G. (1975), *Numerical Models of Ocean Circulation.*, chap. The role of models in tracer studies, pp. 133–146, National Academy of Science.

Waterhouse, A. F., J. A. MacKinnon, J. D. Nash, M. H. Alford, E. Kunze, H. L. Simmons, K. L. Polzin, L. C. St. Laurent, O. M. Sun, R. Pinkel, L. D. Talley, C. B. Whalen, T. N. Huussen, G. S. Carter, I. Fer, S. Waterman, A. C. Naveira Garabato, T. B. Sanford, and C. M. Lee (2014), Global Patterns of Diapycnal Mixing from Measurements of the Turbulent Dissipation Rate., *Journal of Physical Oceanography*, *44*(7), 1854–1872, doi:10.1175/JPO-D-13-0104.1.

Yeager, S. G., and W. G. Large (2008), CORE.2 Global Air-Sea Flux Dataset., *Dataset. http://dx.doi.org/10.5065/D6WH2N0S. Accessed - 26 Mar 2013*, Research Data Archive at the National Center for Atmospheric Research, Computational and Information Systems Laboratory.

Zhurbas, V., and I. S. Oh (2004), Drifter-derived maps of lateral diffusivity in the Pacific and Atlantic Oceans in relation to surface circulation patterns., *Journal of Geophysical Research: Oceans*, *109*(C5), C05,015, doi:10.1029/2003JC002241.

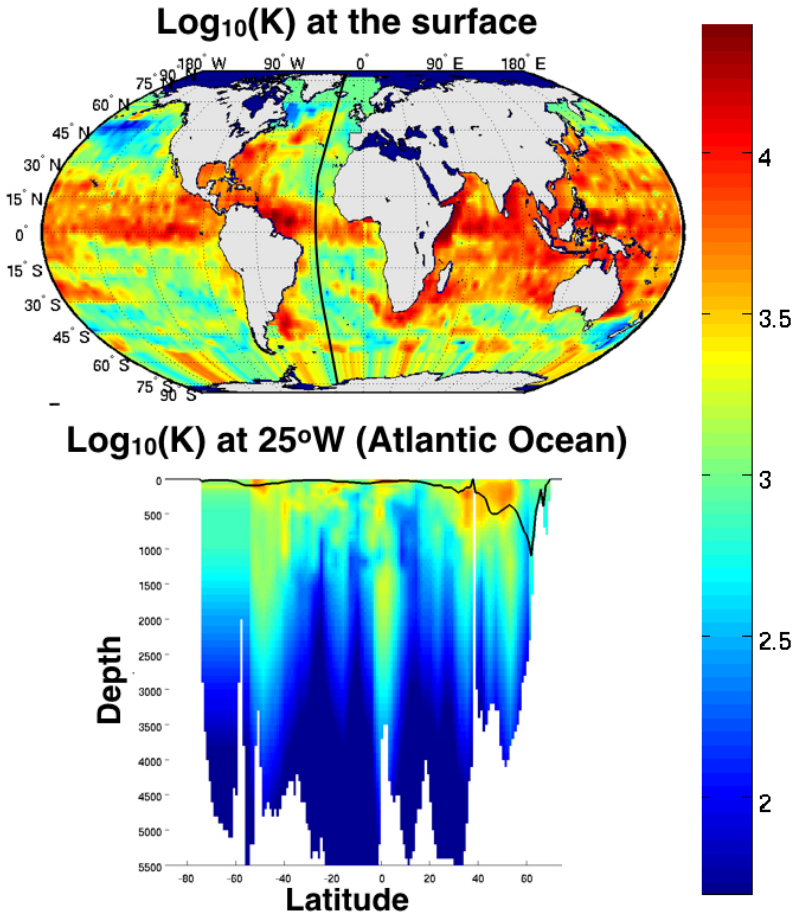

Figure 1. Mesoscale diffusivities K at the surface (top) and at a North-South transect at 25W in the Atlantic (bottom), based on the estimate of *Cole et al.* [2015]. The black line represent the mixed layer depth. The Arctic and inland seas are not available (dark blue in top panel)

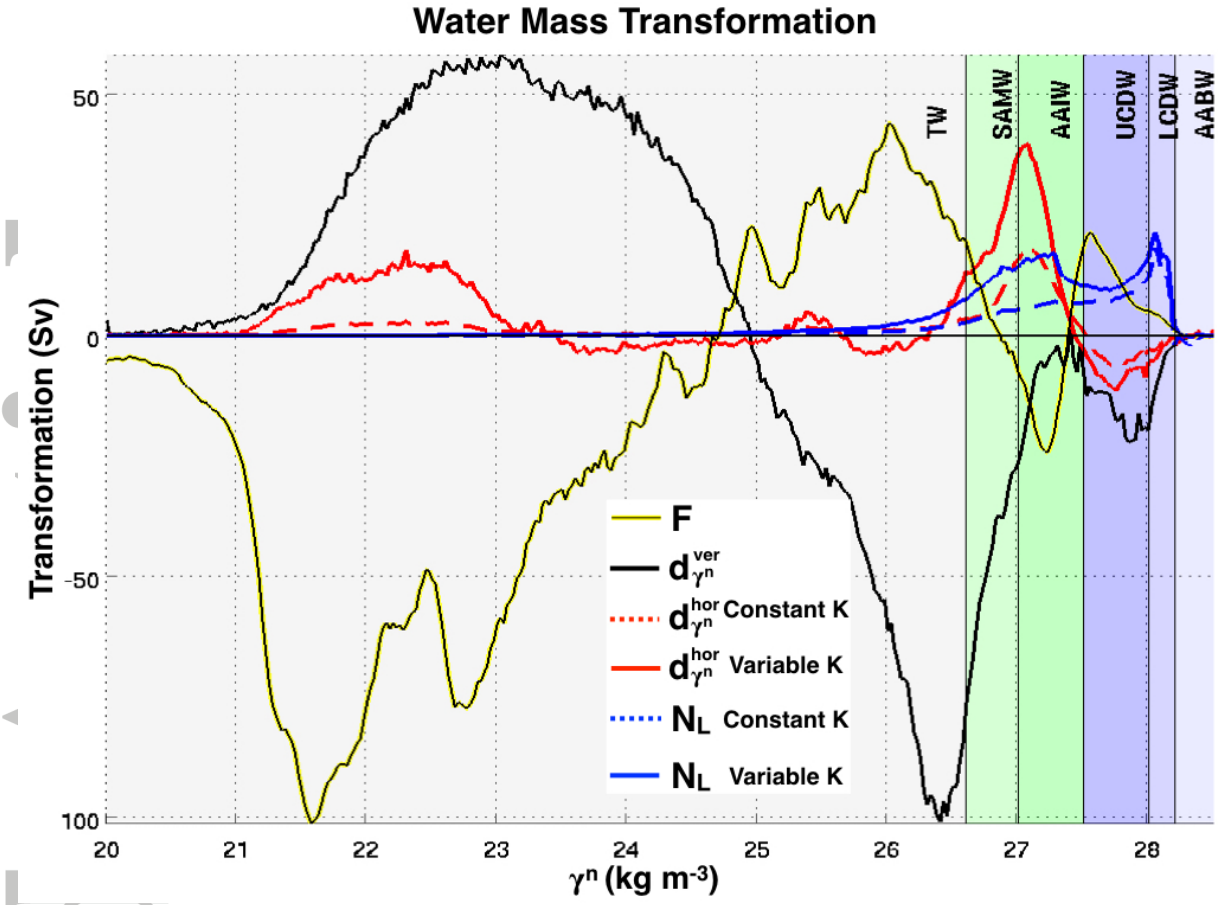

Figure 2. The water mass transformation rates (Sv), as a result of air-sea buoyancy fluxes (yellow), vertical diffusion (black), horizontal diffusion for constant diffusivities (dashed red), horizontal diffusion for spatially varying diffusivities (solid red), NWMT (N_{L}) for constant diffusivities (dashed blue) and NWMT using spatially varying diffusivities (solid blue). The shading and associated abbreviations indicates different water masses, which are Tropical Waters (TW, $\gamma^{\mathrm{n}} < 26.6$ kg m^{-3}), Subantarctic Mode Water (SAMW, $26.6 \leq \gamma^{\mathrm{n}} < 27.2$ kg m^{-3}), Antarctic Intermediate Water (AAIW, $27.2 \leq \gamma^{\mathrm{n}} < 27.5$ kg m^{-3}), Upper Circumpolar Deep Water (UCDW, $27.5 \leq \gamma^{\mathrm{n}} < 28.0$ kg m^{-3}), Lower Circumpolar Deep Water (LCDW, $28.0 \leq \gamma^{\mathrm{n}} < 28.2$ kg m^{-3}) and Antarctic Bottom Water (AABW, $28.2 \leq \gamma^{\mathrm{n}}$ kg m^{-3}).

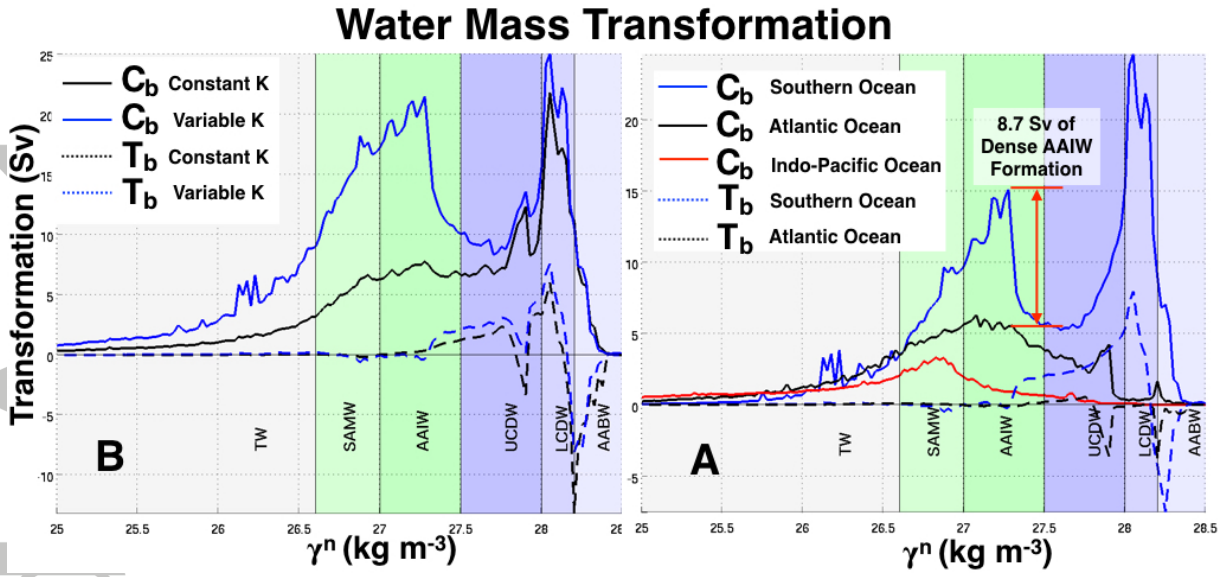

Figure 3. Panel A: Water mass transformation by cabbeling (solid) and thermobaricity (dashed) for constant diffusivities (black, scenario 1) and spatially varying diffusivities (blue, scenario 2). Panel B: Water mass transformation using scenario 2 by cabbeling (solid) and thermobaricity (dashed), split up into contributions from the Southern Ocean (blue), Atlantic Ocean (black) and Indo-Pacific Ocean (red). The Southern Ocean is defined as south of 30°S. Shadings are as in Fig. (2).

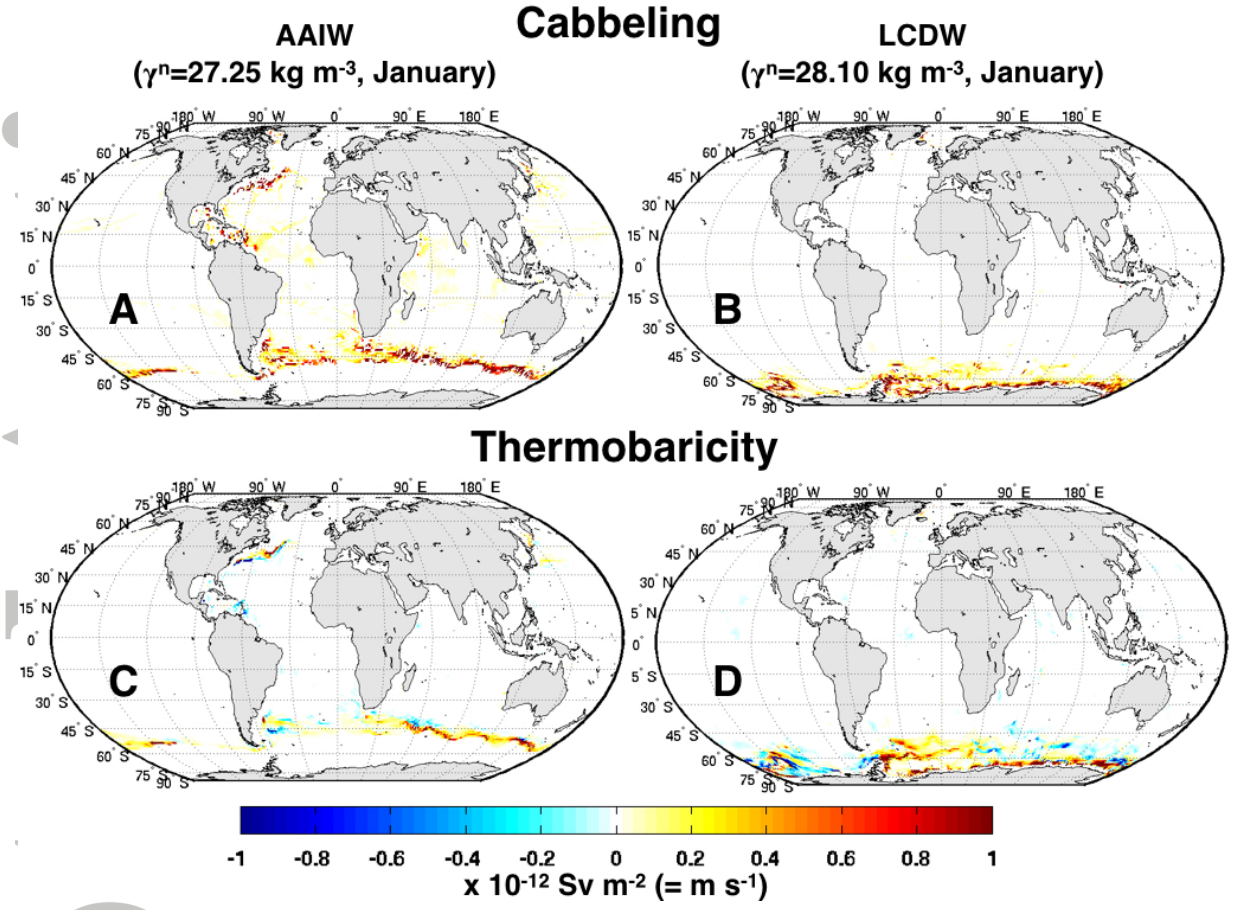

Figure 4. Geographical distribution of water mass transformation in January (Sv m^{-2} = m s^{-1}) by Cabbeling (top, A and B) and Thermobaricity (bottom, C and D), for AAIW (left) and LCDW (right).